AJNR

Magnetic Resonance Imaging in Infants and Children with Spinal Dysraphism

P. D. Barnes, P. D. Lester, W. S. Yamanashi and J. R. Prince

This information is current as of August 6, 2025.

Magnetic Resonance Imaging in Infants and Children with Spinal Dysraphism

P. D. Barnes[1]
P. D. Lester[2]
W. S. Yamanashi[2]
J. R. Prince[1]

Magnetic resonance imaging (MRI) of the spine was used in 37 infants and children to assess the potential of this new technology to evaluate suspected lumbosacral dysraphic myelodysplasia. Eighteen of these patients had correlative metrizamide myelotomography and metrizamide computed tomography (CT). MRI using a spin-echo pulse sequence with short repetition times (TR) and echo delay times (TE) affords optimal delineation of normal and abnormal spinal cord morphology in the lumbosacral region. Coronal projections usually provide an adequate demonstration of the normal conus medullaris for screening purposes; however, multiplanar acquisitions are necessary for more complete delineation of the dysraphic myelopathy. The sensitivity of MRI compares favorably with metrizamide tomography and CT, although these procedures provide somewhat better specificity. These results suggest that MRI is a reliable, noninvasive procedure to screen patients for lumbosacral dysraphism.

There is a need for accurate and noninvasive evaluation of the spine in children suspected to have dysraphic myelodysplasia. While plain-film radiography and sonography are helpful, metrizamide myelography, or myelotomography (MT), and metrizamide computed tomography (MCT) are required for definitive diagnoses [1]. However, these procedures are invasive. New techniques for imaging the spine in children that reduce this risk include new generation CT [2], high-resolution sonography [3, 4], and digital myelography [5].

Since magnetic resonance imaging (MRI) does not involve ionizing radiation, has no known biological risk, and avoids the intrathecal injection of contrast media, it offers several advantages in the evaluation of children with suspected spinal dysraphism [6–9]. We report here our preliminary experience with MRI for this purpose.

Subjects and Methods

In the 16 months between October 1983 and March 1985, 37 patients (21 males and 16 females) between the ages of 8 days and 20 years had MRI of the spine. Twenty-nine of these were suspected of having lumbosacral dysraphic myelodysplasia (Table 1). The MRI findings were correlated with MT and MCT results in 18 patients. Eight normal patients who were studied by MRI served as controls.

The examinations were performed with a Picker MRI machine operating at 0.27 T (11.2 MHz) for the first 31 patients and at 0.5 T (21.3 MHz) for the last six. A spin-echo (SE) pulse sequence was used with repetition times (TR) of 500, 1000, and 2000 msec, and echo-delay times (TE) of 40, 60, 80, and 120 msec. At the 0.27-T field strength, 1-cm single-slice and/or contiguous 1-cm multislice acquisitions were performed. With the 0.5-T field strength, single averaging was used.

A single slice in the axial plane at the T12 level was initially obtained for localization and positioning (Fig. 1). One to four coronal images were then followed by four sagittal images with interval offset readjustments when necessary for repeat acquisition to provide complete spinal cord delineation. Additional axial slices were obtained depending on the clinical indication for the examination and/or the findings from the preceding acquisitions. The decision
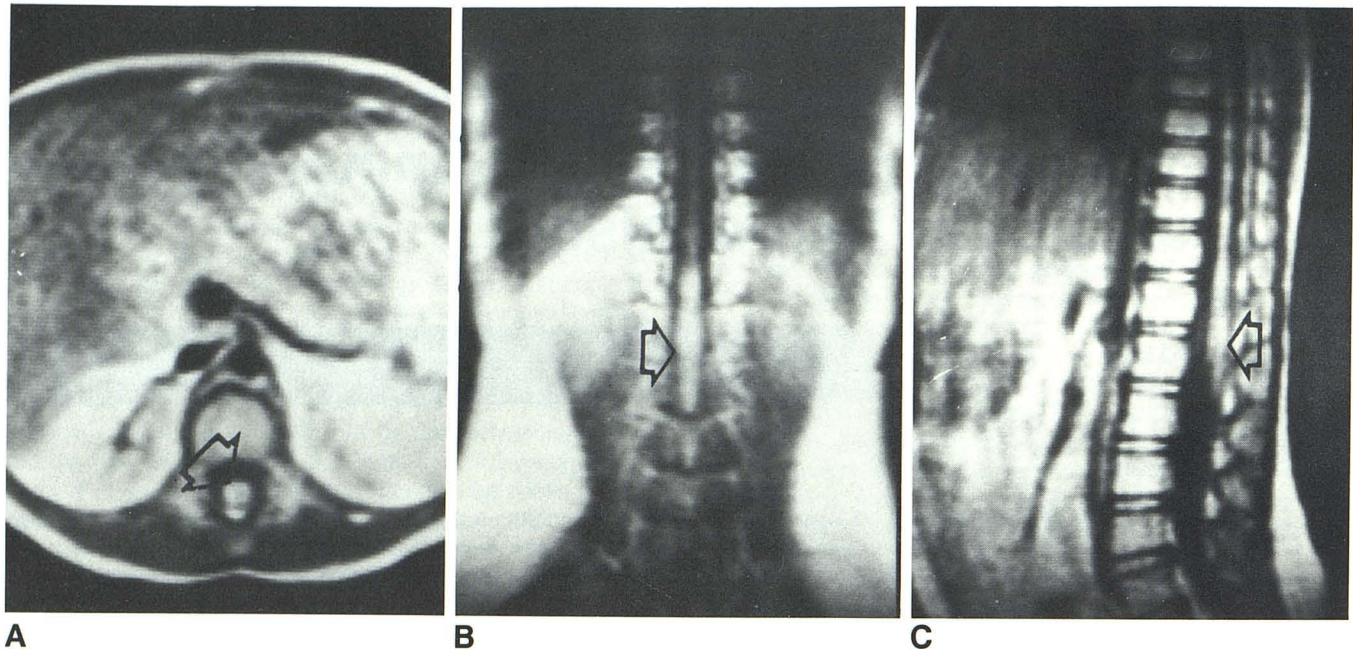
A **B** **C**

Fig. 1.—3-year-old girl, normal control. Transverse (**A**), coronal (**B**), and sagittal (**C**) SE 1000/40 images show higher-intensity normal spinal cord and conus medullaris (*arrows*) contrasted against adjacent, averaged lower-inten- sity extraneural structures. "Pseudoexpansion" of conus (**C**) is related to volume averaging.

TABLE 1: **Clinical and Radiographic Findings with Suspected Dysraphic Myelodysplasia**

Findings	No. of Patients (n = 29)
Clinical:	
Imperforate anus complex	19
Bladder/bowel dysfunction	14
Cutaneous stigmata	12
Limb deformity	8
Congenital scoliosis	8
Vater syndrome	8
Klippel-Feil syndrome	2
Postrepair myelomeningocele	3
Neurofibromatosis	1
Radiographic:	
Sacral dysgenesis	9
Lumbosacral dysraphism	13
Congenital scoliosis	8
Craniocervical anomaly	2
Spina bifida occulta	4
Normal plain film	9

to use either the single-slice or multislice technique was guided by the patient's size and the type of spinal curvature as revealed by plain radiographs.

The lower thoracic and lumbosacral spine was examined in all patients. Eight patients also had upper thoracic and craniocervical studies. Correlative MT was performed by using the Philips U3 Polytome, and MCT was performed with either the Varian V-360-3, the Philips Tomoscan 350, or the General Electric CTT 9800.

When necessary, patients were sedated, with chloral hydrate orally for infants less than 2 years old and with intramuscular meperidine and phenergan for children less than 6 years old. When needed, a body wrap was used to immobilize children less than 4 years old.

The children were studied in the supine or lateral decubitus position, and either a 25-cm or 50-cm RF body coil was used. Visual and cardiac monitoring were employed, and a pneumatic hand alarm was available. Parents attended their children during the examinations, which ranged from 30 to 105 min in duration.
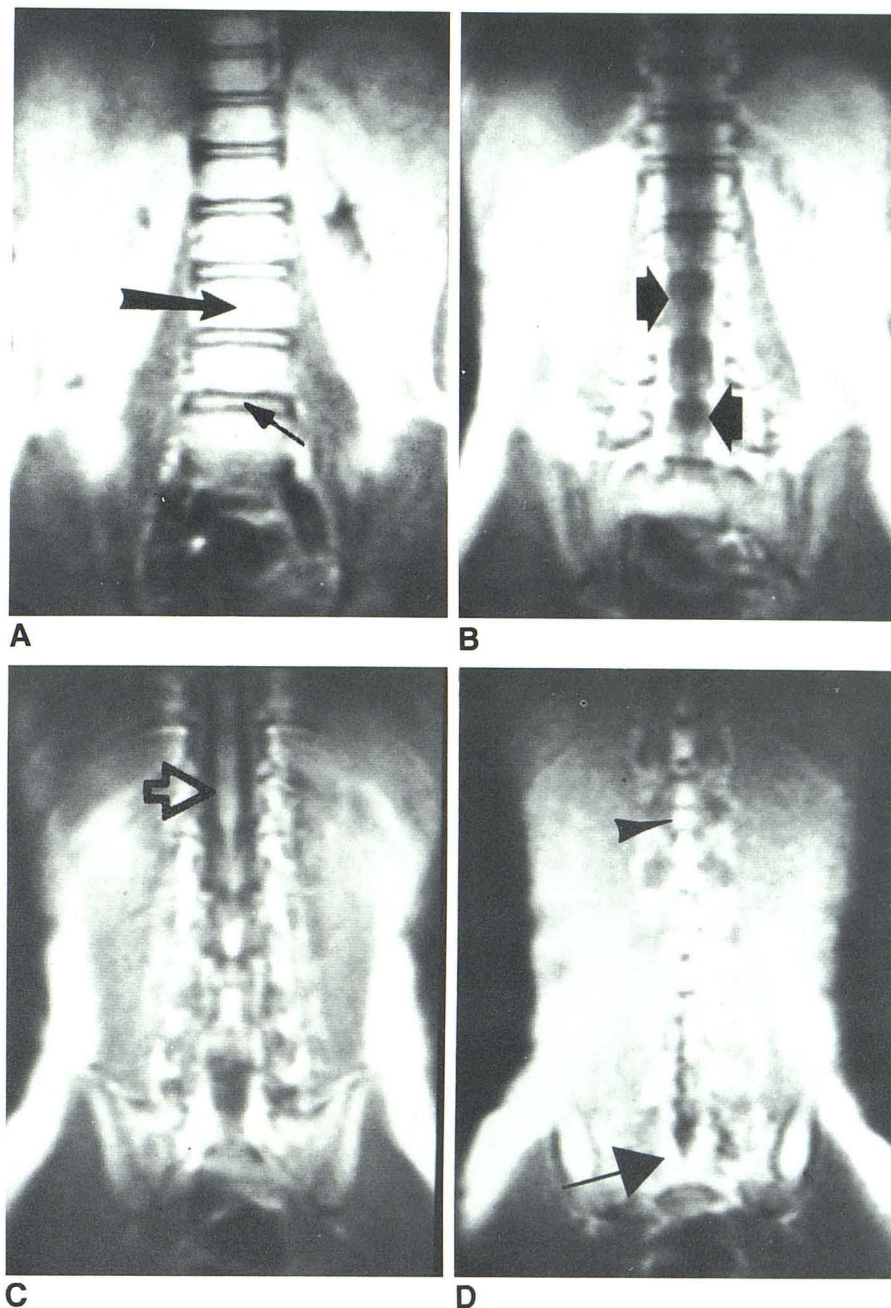
Results

Normal Anatomy

A normal MRI study was defined as one demonstrating a normal conus medullaris located above the intervertebral space between the second and third lumbar vertebrae [2]. The spinal cord in the lower thoracic and lumbar region is best demonstrated by using a short TR (500–1000 msec) and short TE (40 msec) pulse sequence providing a T1-weighted image.

The spinal cord appears as an intermediate- to high-intensity tubular structure that tapers caudally into the conus medullaris at the level of the upper lumbar vertebrae (Figs. 1 and 2). The spinal cord is distinct from the lower-intensity cerebrospinal fluid (CSF), dura mater, longitudinal ligaments, cortical margins of the vertebral bodies and neural arches, and annulus fibrosus of the intervertebral disks. These structures, in turn, are sharply contrasted against the relatively high signal intensity of the epidural fat, the bone marrow of the adjacent skeleton, and the nucleus pulposus of the intervertebral disks. SE pulse sequences with longer TR (1500–2000 msec) and longer TE (60–120 msec), which are primarily proton density and T2-weighted, create images in which the spinal cord is obscured by the high signal of the CSF.

Fig. 2.—6-year-old boy, normal control. Coronal SE 1000/40 images, anterior to posterior. **A**, Anterior section through vertebral bodies (*long arrow*) and disk spaces (*short arrow*). **B**, Through anterior dural sac (*arrows*). **C**, Through posterior dural sac, spinal cord, and conus medullaris (*arrow*). **D**, Posterior section through neural arches, epidural fat (*arrow*), and epidural fat between ligamentum flavum (*arrowhead*).

Of the studies in 29 patients and 8 normal controls, 29 were judged to be of good-to-excellent quality, and eight studies were of fair-to-poor quality. Four of these were nondiagnostic. Four of the poor-quality studies resulted from inability to immobilize the patient properly despite sedation, and four nondiagnostic examinations were related to patient noncompliance.

The ability to determine the position of the conus medullaris was judged to be adequate on either the coronal or sagittal sections in 24 of 27 patients. The conus was best seen on the coronal sections in 20 of 24 patients (Fig. 2), even though exaggerated spinal curvatures made optimum delineation difficult in 11 patients (Fig. 3). Volume averaging of the conus

with the proximal cauda equina occasionally produced a false appearance of an expanded conus on sagittal sections (Fig. 1). Adequate visualization of the conus was also particularly difficult when it was posteriorly placed and/or flattened in the sagittal plane, and when there was an accentuated lumbar lordosis or thoracic kyphosis. In these situations, volume averaging of the conus medullaris and cauda equina nerve roots on images in the sagittal plane occasionally produced the false impression of an abnormally low-placed conus (Fig. 4), particularly with longer TR and TE sequences. Also, respiratory and bowel-motion artifacts in the direction of the phase-encoding gradient often obscured anatomic detail in the sagittal planes.
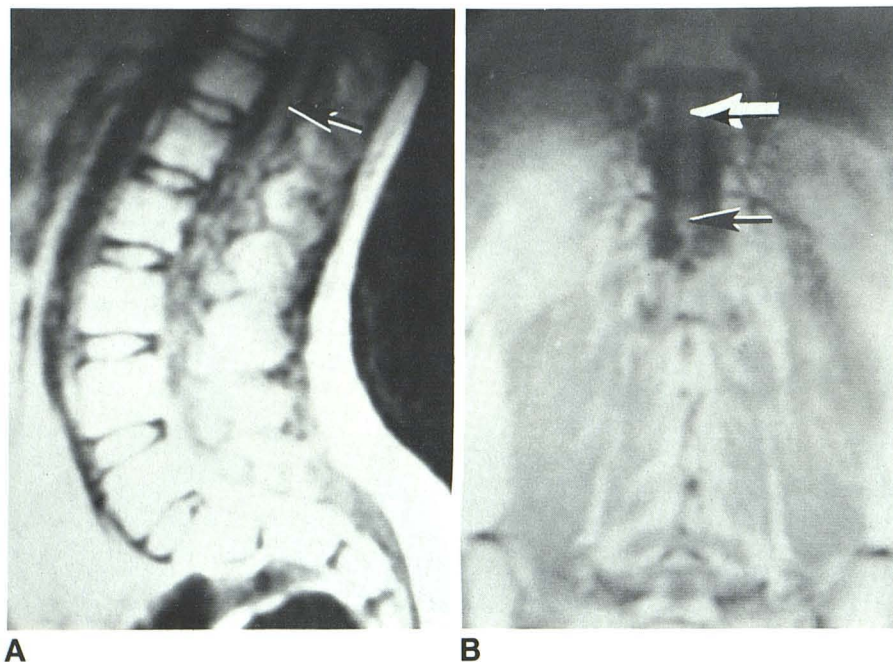
Fig. 3.—15-year-old girl. SE 1000/40 sagittal (**A**) and coronal (**B**) images show exaggerated lumbar lordosis effect on delineation of normal conus medullaris (*arrows*).
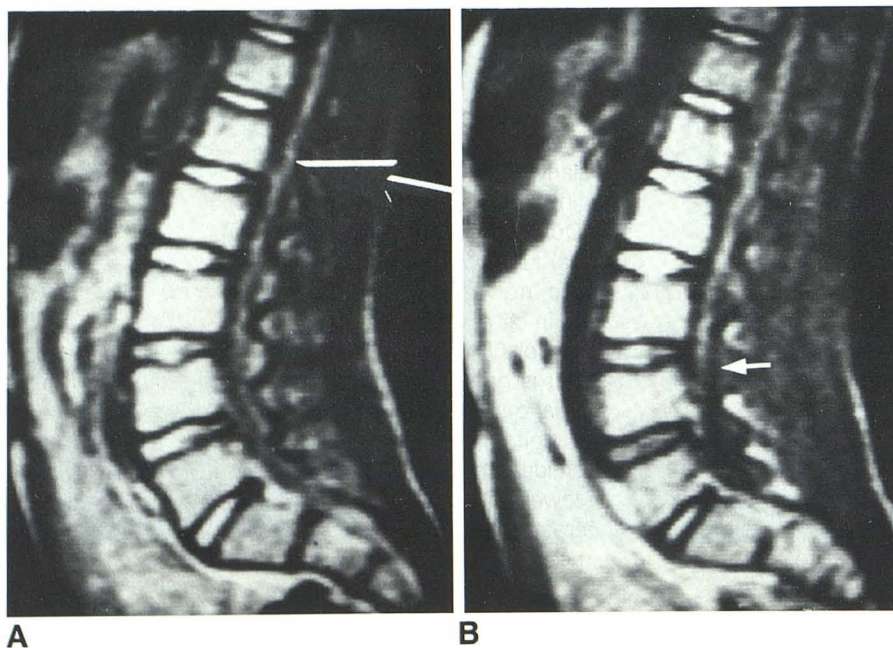

Fig. 4.—14-year-old boy with normal myelotomogram and metrizamide CT scan. SE 2000/40 sagittal images show volume averaging of normal conus and cauda equina giving false impression of tethered cord (*arrows*).

Myelodysplasia Findings

The results for 18 patients who were evaluated for suspected myelodysplasia with correlative MT and MCT are listed in Table 2. These include 10 patients with abnormalities of the lower neuraxis, two with upper neuraxis lesions, and six with normal results. Of the patients without correlative imaging to date, the MRI was considered "probably" normal in

seven and nondiagnostic in four, as above mentioned.

In all 18 patients, MRI reliably distinguished normal from abnormal spinal cord morphology. Again, normal conus position and morphology were best demonstrated on coronal sections (eight patients). In the 10 patients with lower neuraxis myelodysplasia, the abnormally low conus was better delineated on sagittal sections (8 of 10), primarily because of the lordotic lumbosacral curvature effect on coronal plane sec-
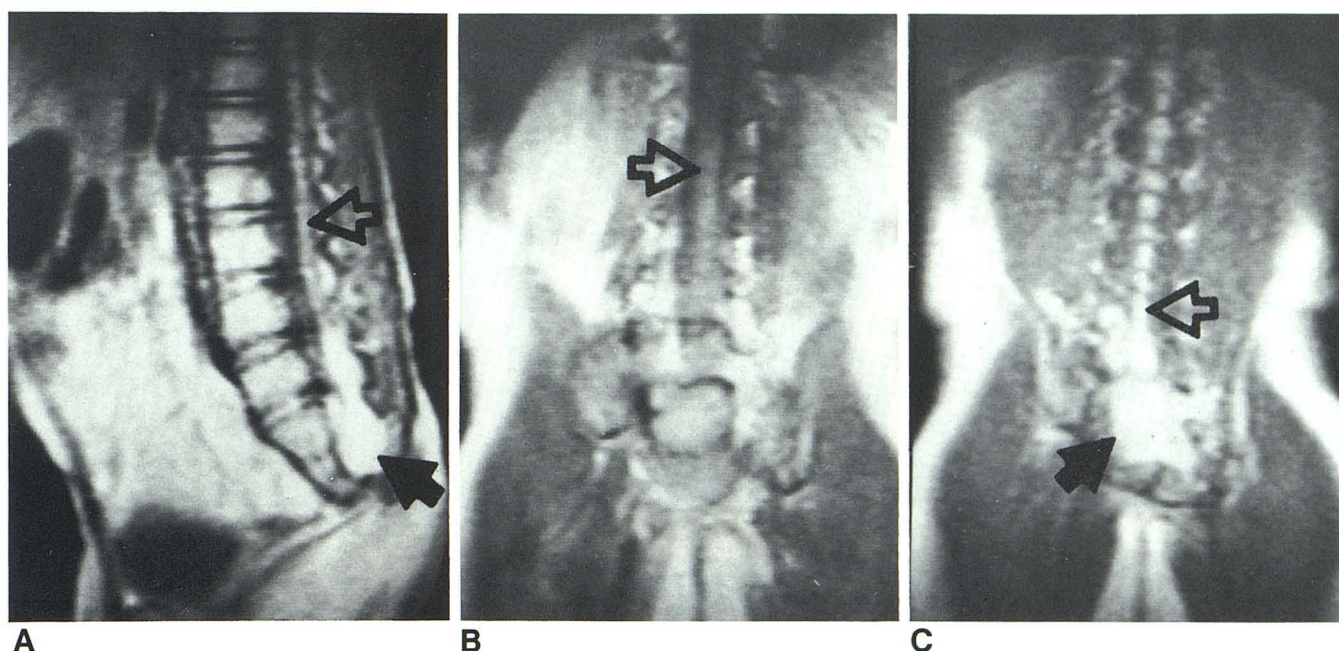
Fig. 5.—5-year-old boy with lipomeningocele. Sagittal SE 1000/40 (**A**) and coronal SE 2000/40 (**B** and **C**) images. Low-placed spinal cord (*open arrow*) with caudal, high-intensity expansion (*solid arrows*) shown to better advantage on sagittal section.

TABLE 2: **Pathologic Findings with Correlative MRI, MT, and CT**

Findings	No. of Patients (n = 18)
Dysplastic conus medullaris	2
Tethered conus with lipomas	2*
Lipomeningocele	2*
Diastematomyelia	1*
Lipomyelocystocele	1*
Postrepair myelomeningocele tethered cord	2*
Cervical diplomyelia with normal conus	1
Cervical syringohydromyelia with normal conus	1*
Normal conus medullaris	6

* Surgical pathology correlation.

tions (Fig. 5). Coronal, sagittal, and often transverse sections were necessary for more complete characterization of the abnormalities, including such associated lesions as developmental masses (Fig. 6), saccular or cystic components (Fig. 7), and diastematomyelia (Fig. 8).

Even though MRI demonstrated the myelodysplastic abnormalities with a sensitivity equal to that of MT and MCT, the latter combination was superior in all cases for spatial delineation of cord and nerve root morphology as well as demarcation of associated component anomalies, including identification of fatty lesions and bony defects (Fig. 6). However, in all patients, MT and MCT required intrathecal injections and heavy sedation in addition to the attendant radiation dose associated with polytomographic and high-resolution CT techniques.

Discussion

The application of MRI for evaluation of spine disease, and particularly spinal dysraphism, in children has received encouraging, though limited, attention in the imaging literature [8, 9]. Our study addresses proton imaging of the normal and abnormal lumbosacral neuraxis in patients with suspected dysraphic myelodysplasia, an important cause of neurologic disability in childhood [10].

High-resolution sonography has proved useful for screening, but it is presently restricted to infants or older patients with spinal defects that provide a bony window [3, 4]. Subtraction digital myelography has been used successfully for metrizamide examination, but its application has been limited to the lower neuraxis of infants and young children because of contrast medium dilution and motion difficulties [5]. Until now, metrizamide myelography and CT have been the most reliable combination of techniques for definitive presurgical evaluation. These procedures are currently superior to all other techniques, including MRI, for the demonstration of the cauda equina and filum terminale; the location of placode, fat, and nerve roots; and the indication of the presence of osseous, cartilaginous, or fibrous bands dividing the dura in diastematomyelia.

MRI, which is noninvasive and has superb contrast resolution, may be an excellent screening technique for lumbosacral dysraphism, as suggested by the findings in this limited series. With further application, experience, and technological development, MRI may become a cost-effective method for complete pretherapy evaluation and follow up.

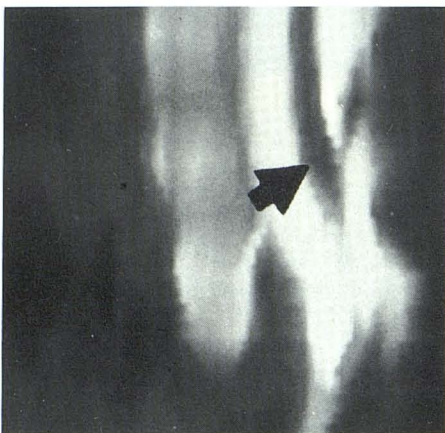Short TR/TE pulse sequences with coronal multislice ac-
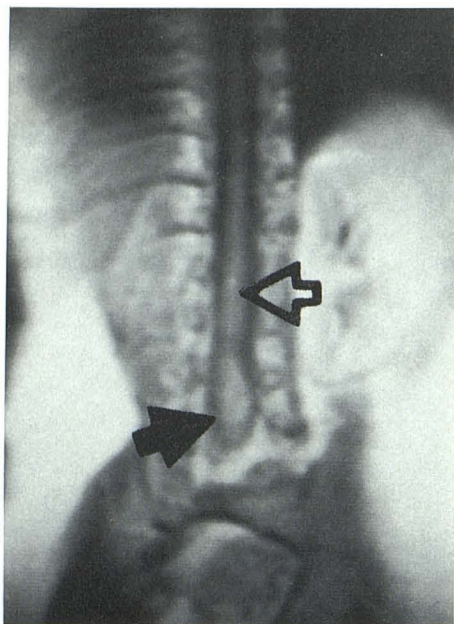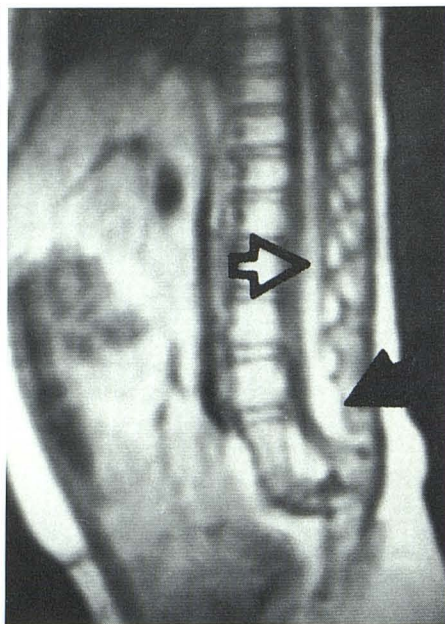
Fig. 6.—2-year-old boy; tethered cord with lipomas. SE 1000/40 coronal (A) and sagittal (B) slices. Low-placed cord (*open arrows*) and caudal, high-intensity mass (*solid arrows*). Frontal myelotomogram (C) provides clearer demarcation of the lipomas (*arrows*), while axial (D) and sagittal (E) reformatted metrizamide CT provides more specific fat-density characterization (*arrow*).
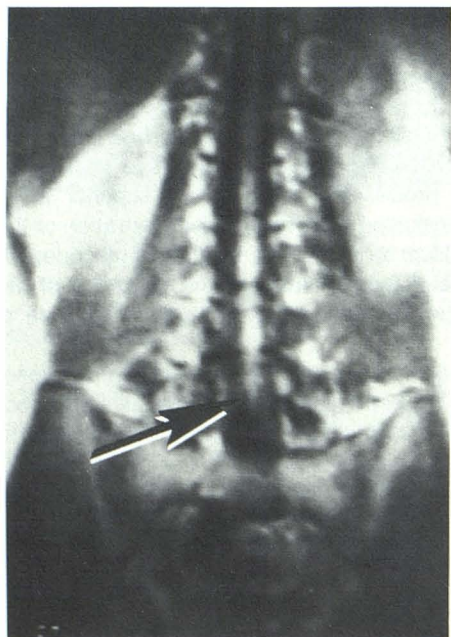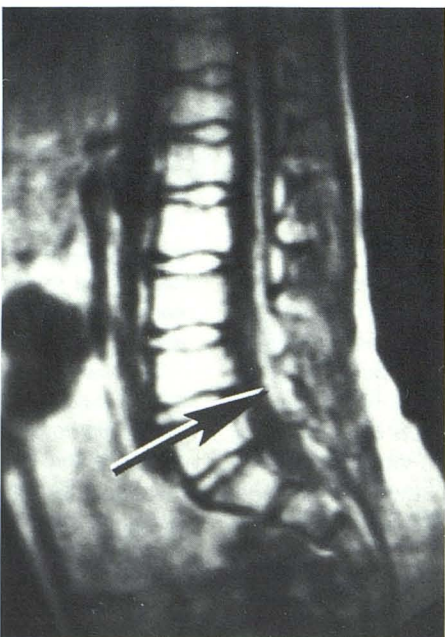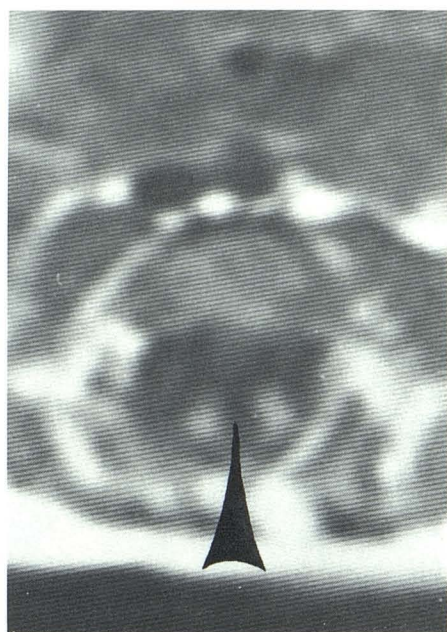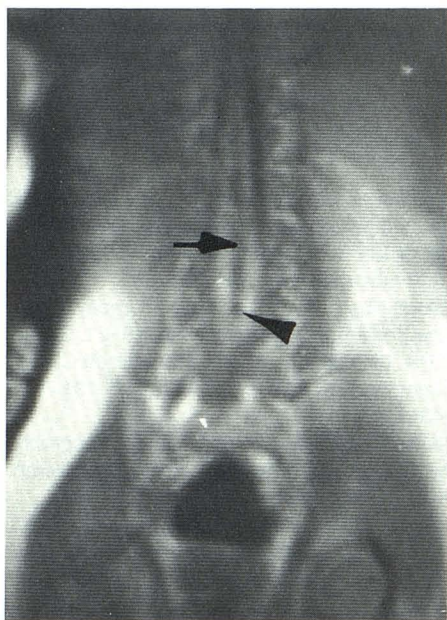

Fig. 7.—9-year-old boy postmyelomeningocele repair; tethered cord. SE 1000/40 coronal (A) and sagittal (B) slices showing low-placed, thinned cord and conus placode within the caudal sac (*arrow*).
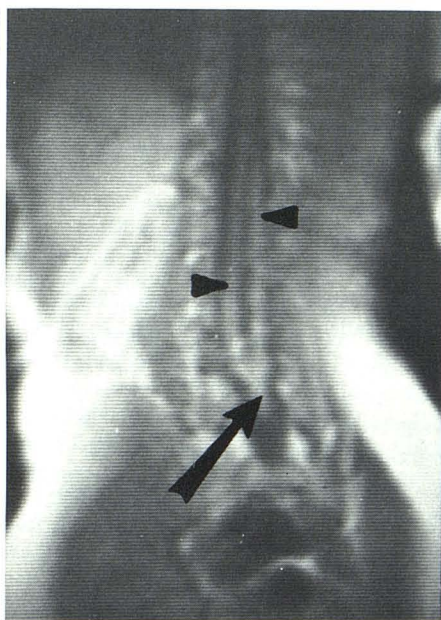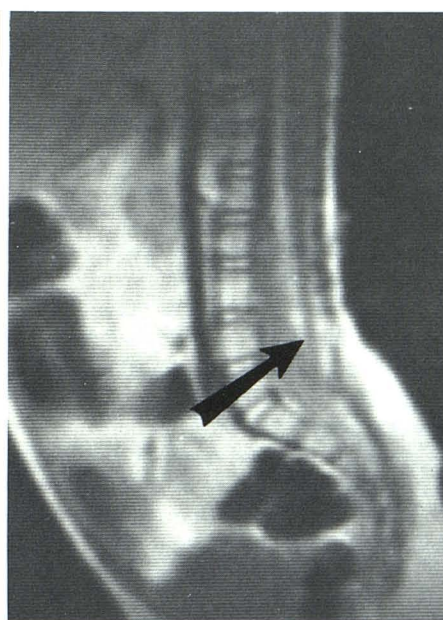
Fig. 8.—18-month-old girl; diastematomyelia. SE 1000/40 transverse (**A**), coronal (**B** and **C**), and sagittal (**D**) images show intermedullary defect (*short arrows*), hemicords (*short arrowheads*), low conus (*long arrow*), and focal signal dropout of cortical bony septum (*long arrowhead*).

quisition provide the most efficient way to obtain optimal demonstration of conus morphology. Sagittal imaging may also be required in the presence of spinal curvatures. Multiplanar imaging that uses these pulse sequences affords more complete characterization of the myelopathy in patients with dysraphic myelodysplasia.

The T1-weighted technique provides good anatomic delineation because the high-intensity neural structures are well seen adjacent to the low-intensity extraneural tissues, although nerve roots and the filum terminale have not been reliably or consistently demarcated. On T2-weighted images,

the high signal intensity of the cerebrospinal fluid tends to obscure the neural tissues. However, these images assist in the delineation of extradural bony and soft-tissue components.

Increasing the field strength from 0.27 T to 0.5 T allows a significant reduction in the imaging time while improving image quality. However, the 1-cm slice thickness remains a major limiting factor in the spatial resolution of neural landmarks because of volume averaging. Technical improvements to allow thin-slice, high-resolution capabilities [11] (Fig. 9) will help to separate medium- to high-intensity neural structures
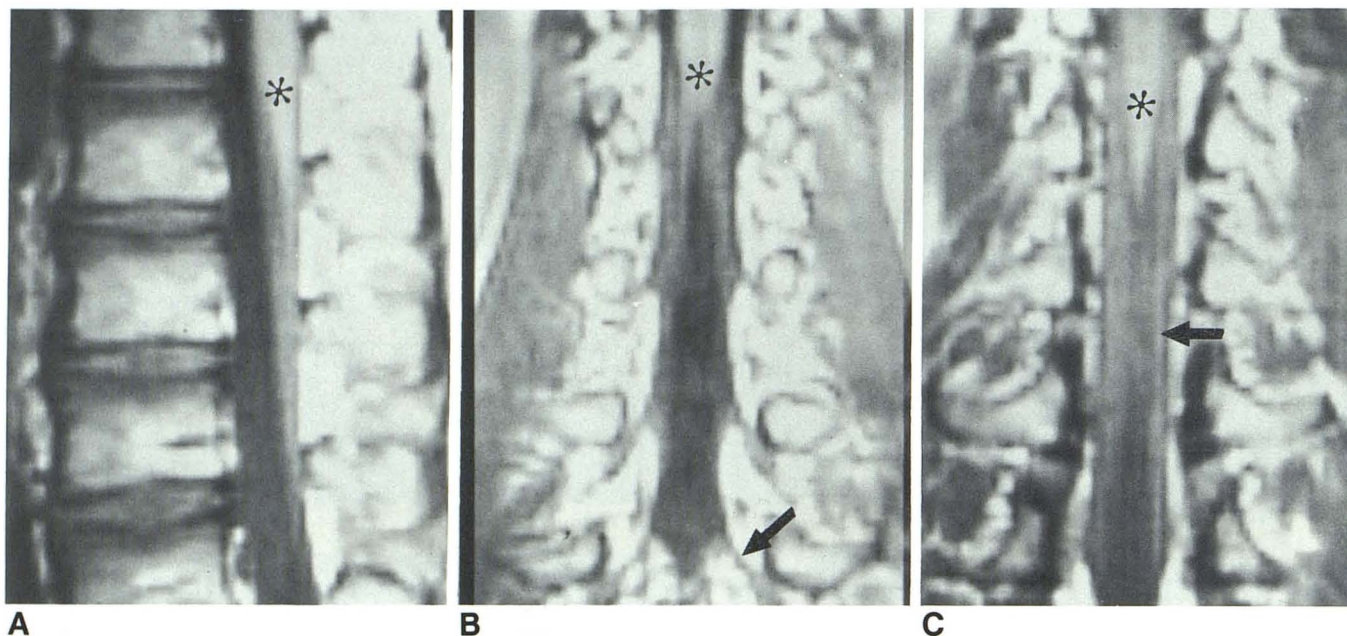
A　　　　　　　　　　　　　　　　B　　　　　　　　　　　　　　　　C

Fig. 9.—9-year-old girl; normal lumbosacral sagittal (A) and coronal (B and C) MRI at 1.5 T using 13.75-cm surface coil and partial saturation 400/25, 256 × 256 matrix, 32-cm FOV, and 3-mm slice thickness demonstrating conus (*) separated from cauda equina with definition of nerve roots (arrow) (C) and axillary sleeves (B). Courtesy PDB, ODI Inc., Oklahoma City, OK, and GE Medical Systems, Milwaukee, WI.

from high-intensity nonneural component abnormalities (i.e., lipomatous lesions) and also to demonstrate cord thinning related to myelomalacia or collapsed hydromyelia.

Several factors are particularly important in MRI of the spine in children. Careful positioning and localization are critical to overcome spinal curvature difficulties. Plain radiographs and preliminary transverse single slices have been helpful, but occasionally coronal or sagittal preacquisition single slices are needed to correct or avoid off-axis imaging. Careful application of an abdominal compression band has significantly reduced respiratory and bowel-motion artifacts, particularly in infants. Patient compliance is mandatory, and in general there has been good acceptance of the MRI procedure by both parents and children, particularly when there is good preparation and an informed understanding of the procedure as compared with more invasive alternatives. With increased experience, fewer children have required sedation, particularly when examined after feedings and when accompanied by the parent.

At present, our suggested approach for evaluating clinically suspected lumbosacral dysraphism after reviewing plain spine films includes high-resolution sonography (accessible window) and/or MRI for screening normal conus morphology and level. MT and MCT are then recommended for those cases in which MRI is equivocal or incomplete.

REFERENCES

1. Barnes, PD. Progress in cost-effective radiologic evaluation of pediatric and adolescent neurologic spine disease. Presented at the annual meeting of the Society for Pediatric Radiology, Atlanta, April 1983, AJR (abstract) 1983;141:851–852
2. Petterson H, Harwood-Nash DC. CT and myelography of the spine and cord. New York: Springer-Verlag, 1982:9–21, 32–33
3. Kangarloo H, Gold RH, Diament MJ, Boechat MI, Barrett C. High resolution spinal sonography in infants. AJNR 1984;5:191–195, AJR 1984;142:1243–1247
4. Naidich TP, Fernbach SK, McLone DG, Shkolnik A. Sonography of the caudal spine and back: congenital anomalies in children. AJNR 1985;5:221–234, AJR 1984;142:1229–1242
5. Barnes PD, Reynolds AF, Galloway DC, Pollay M, Leonard JC, Prince JR. Digital myelography of spinal dysraphism in infancy: preliminary results. AJNR 1984;5:208–211, AJR 1984; 142:1249–1252
6. Lester PD, Barnes PD, Yamanashi WS, Maulsby GO. Magnetic resonance imaging in infants and children with spinal dysraphism. Presented at the annual meeting of the Society for Pediatric Radiology, Las Vegas, April 1984, AJR (abstract) 1984;143:694
7. Norman D, Mills CM, Brant-Zawadzki M, Yeates A, Crooks LE, Kaufman L. Magnetic resonance imaging of the spinal cord and canal: potentials and limitations. AJNR 1984;5:9–14, AJR 1983;141:1147–1152
8. Han JS, Kaufman B, Yousef SJE, et al. NMR imaging of the spine. AJNR 1983;4:1151–1160, AJR 1983;141:1137–1145
9. Modic MT, Weinstein MA, Pavlicek W, Starnes DL, Duchesneau PM, Boumphrey F, Hardy RJ. Nuclear magnetic resonance imaging of the spine. Radiology 1983;148:757–762
10. Sarwar M, Virapongse C, Bhimani S. Primary tethered cord syndrome. AJNR 1984;5:235–242
11. Edelman R, Shoukimas G, Stark D, et al. High-resolution surface-coil imaging of lumbar disk disease. AJNR 1985;6:479–485